Curvature-induced anisotropic spin-orbit splitting in carbon nanotubes

L. Chico, M. P. López-Sancho, and M. C. Muñoz
Instituto de Ciencia de Materiales de Madrid, Consejo Superior de Investigaciones Científicas, Cantoblanco, 28049 Madrid, Spain
(Received 22 February 2009; revised manuscript received 5 May 2009; published 19 June 2009)

We have theoretically explored the spin-orbit interaction in carbon nanotubes. We show that, besides the dependences on chirality and diameter, the effects of spin-orbit coupling are anisotropic: spin-orbit splitting is larger for the higher valence or the lower electron band depending on the specific tube. Different tube behaviors can be grouped in three families, according to the so-called chiral index. Curvature-induced changes in the orbital hybridization have a crucial role, and they are shown to be family dependent. Our results explain recent experimental results which have evidenced the importance of spin-orbit effects in carbon nanotubes.

DOI: 10.1103/PhysRevB.79.235423 PACS number(s): 71.20.Tx, 73.22.−f, 71.70.Ej

I. INTRODUCTION

Improvements in the quality of carbon nanotubes (CNTs) have enabled the fabrication of quantum dots (QDs) aiming at the realization of spintronics devices.[1–4] CNTs present a high Fermi velocity and a twofold orbital degeneracy originating from the topology of the honeycomb lattice. The unique fourfold degeneracy of CNT energy states (spin plus orbital moment) has been observed in CNT QDs by magnetic field spectroscopy measurements[5] and makes them particularly interesting since, besides the spin degree of freedom, they present the orbital moment to allow for quantum manipulation. In a recent experiment,[6] spin-orbit (SO) coupling has been directly observed in CNTs as a splitting of the fourfold degeneracy of a single-electron energy level in ultraclean QDs. This important finding seems to be in contradiction with the interpretation of earlier experiments in defect-free CNTs, from which independent spin and orbital symmetries and electron-hole symmetry have been deduced.[7] Besides showing the importance of spin-orbit effects in carbon nanotubes, Kuemmeth *et al.*[6] pointed out an unexplained anisotropic splitting of electron and holes in carbon nanotube quantum dots, which deserves further exploration.

In an earlier work, we showed that the inclusion of the full lattice symmetry is essential for deriving SO effects in CNTs.[8] Employing an empirical tight-binding (ETB) model, we demonstrated an intrinsic symmetry dependence of spin-orbit interaction (SOI) effects. As confirmed by recent experimental results,[6] we showed that, in the absence of a magnetic field, CNTs present spin-orbit split bands at the Fermi level. In addition, SOI induces zero-field spin splitting in chiral CNTs, while Kramers theorem on time-reversal symmetry alongside the spatial inversion symmetry preserves the spin degeneracy in achiral—i.e., (n,n) armchair and $(n,0)$ zigzag—nanotubes.[9] Because of the small value of SOI in carbon atoms, its effects were previously investigated on CNTs by deriving an effective-mass Hamiltonian with a weak SOI in carbon orbitals to the lowest order in perturbation theory.[10] Band splitting was found considering surface-curvature effects,[11] as well as in the electron-spin-resonance spectra of achiral CNTs derived by low-energy theory.[12] More recent works[13] have indicated the importance of curvature of SOI effects in graphene, fullerenes, CNTs, and NT caps investigated with a continuum model by perturbation theory, reporting the appearance of a gap and spin splitting in the CNT band spectrum due to SOI. Three effective SO couplings are derived (intrinsic, curvature, and electric field) from the intra-atomic SO coupling for a continuum model of the graphene π bands at the K and the K' points of the honeycomb lattice Brillouin zone (BZ).[13] These authors extend the graphene continuum model to CNTs, considering the SO interaction in a cylinder; by integrating over the tube circumference, the SO term is obtained at the K and the K' points of the CNT. Moreover, SOI effects have been recently studied in CNT quantum dots.[14,15] Starting from the graphene Dirac Hamiltonian and taking into account the intrinsic SO mechanism[16] and the extrinsic SOI (Bychkov-Rashba type) of graphene, SOI effects are derived for CNTs, finding a level splitting at zero magnetic field.[14] In Ref. 15 SOI effects are found to intrinsically lift the fourfold degeneracy of a single electron in a CNT quantum dot studied in the low-energy limit.

Here we show that, besides the dependences on the diameter and the chirality, SOI effects in CNTs exhibit an electron-hole anisotropy which is specific to the tube. Distinct nanotube behaviors with respect to SOI are grouped into three families, which have also arisen with respect to other electronic properties.[17] We relate such differences to changes in hybridization of the valence and the conduction bands (CBs) in nanotubes belonging to different families.

The paper is organized as follows. In Sec. II the theoretical model is presented and results are discussed in Sec. III. Finally, our conclusions are given in the last section.

II. MODEL AND METHOD

We have performed a Slater-Koster (SK) (Ref. 18) ETB calculation employing a four-orbital $2s,2p_x,2p_y,2p_z$ basis set using the Tománek-Louie parametrization for graphite.[19] The CNT unit cell is formed by rolling up a portion of a graphene sheet; thus, the actual discrete nature of the lattice and curvature effects are taken into account.

The spin-orbit interaction arises from the coupling of the electron spin with the magnetic field resulting in the rest frame of the electron due to its orbital motion in an electrostatic potential V. The SO coupling term in the Hamiltonian is given by

$$H_{\mathrm{SO}} = \frac{\hbar}{4mc^2}\boldsymbol{\sigma}\cdot(\nabla V \times \mathbf{p}), \tag{1}$$

where $\boldsymbol{\sigma}$ represents the Pauli spin matrices and $\mathbf{p}$ represents the electron momentum operator. Equation (1) stems from the quadratic v/c expansion of the Dirac equation and represents a nonrelativistic approximation to the relativistic Dirac equation.

In a crystalline environment, in the absence of external fields, the major internal contribution to V arises from the microscopic crystal potential. Thus, the magnetic field acting on the electron is modified by the presence of neighboring atoms, and therefore its effects are related to the crystal symmetry. However, the relevant contribution of the crystal potential for the spin-orbit interaction is close to the atomic cores, so one can assume spherical symmetry. In this way, SO effects are considered by adding to the SK-ETB spin-independent Hamiltonian H_0 the atomiclike spin-orbit term

$$H_{\mathrm{SO}} = \lambda \mathbf{L}\cdot\boldsymbol{\sigma}, \tag{2}$$

where λ is a renormalized atomic SO coupling constant and $\mathbf{L}$ stands for the orbital angular momentum of the electron. The spin-quantization direction z has been chosen parallel to the carbon nanotube axis. Employing the raising and the lowering operators, $L_+ = L_x + iL_y$, $L_- = L_x - iL_y$, the complete Hamiltonian of a nanotube with N atoms in the unit cell, $H = H_0 + H_{\mathrm{SO}}$, is a matrix of dimensions $8N \times 8N$, which in the 2×2 block spinor structure is given by

$$H = \begin{pmatrix} H_0 + \lambda L_z & \lambda L_- \\ \lambda L_+ & H_0 - \lambda L_z \end{pmatrix}. \tag{3}$$

The H_{SO} term of the Hamiltonian couples states of equal angular momentum in the same atom,[20,21] i.e., p orbitals in the present case. We solve the problem by direct diagonalization of the Hamiltonian matrix. Although our discussion is focused in the bands around the Fermi level, our calculation is valid for the full band structure, in contradistinction to the effective-mass model.

The spin-orbit interaction considered in our model is the so-called intra-atomic spin-orbit interaction; extrinsic effects due to external potentials are not considered here. The H_{SO} term in the Hamiltonian includes all the spin contributions arising from the NT crystal potential. Therefore, it contains the intrinsic Δ_{int} and the curvature Δ_{curv} contributions of the effective spin-orbit Hamiltonian derived by perturbation theory.[10,13]

Different estimations of λ have been done,[10,13] always assuming a very small value, considerably reduced in graphite/graphene and CNTs with respect to the value for atomic C ($\approx$12 meV). However, the recent experiments of Ref. 6 point out an enhancement of the role of SOI in CNTs with respect to that of graphene; thus, the exact value of the SO coupling parameter is still under discussion. In the present work, SO-induced energy splittings are given relative to the strength of the SOI, and only in band-structure results we have chosen an artificially large value of λ, for the sake of clarity in the figures.

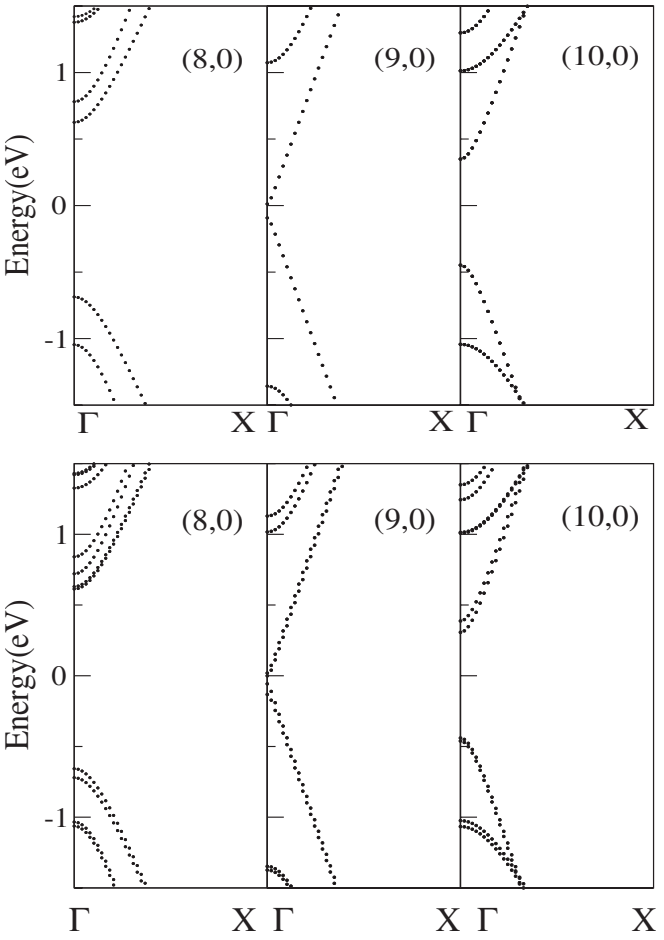

FIG. 1. Band structures calculated around the Fermi level for three zigzag CNTs: (8,0) tube from the $(3q-1,0)$ family, (9,0) primary metallic nanotube from the $(3q,0)$ family, and (10,0) tube from the $(3q+1,0)$ series. The top panel shows the results without including SO effects; the band structures of the bottom panel have been calculated including the SOI term with $\lambda = 0.2$ eV.

III. RESULTS

A. Achiral tubes

We focus first on achiral zigzag nanotubes with a chiral angle $\theta = 0°$, where curvature effects are expected to be largest.[22,23] Zigzag $(n,0)$ tubes can be classified as primary metals[23] if $n = 3q$, with q being an integer, or semiconducting, if $n = 3q \pm 1$. Without curvature effects, primary metallic zigzag tubes have a band crossing at the Fermi level; this occurs at the center of the BZ. The bands crossing at Γ are fourfold degenerate, and inclusion of curvature opens a small gap. Zigzag tubes with $n = 3q \pm 1$ are semiconducting with the band gap at Γ; the top valence and the bottom conduction bands are also fourfold degenerate.

Inclusion of SO interaction partially removes the band degeneracy, although the split bands remain spin degenerate, i.e., the SO coupling lifts the fourfold degeneracy into two Kramers doublets. However, the energy splittings induced by the SO interaction term are different for the highest valence band (VB) and the lowest CB: in two of the families, for CNTs $(3q,0)$ and $(3q-1,0)$, the splitting is larger for the

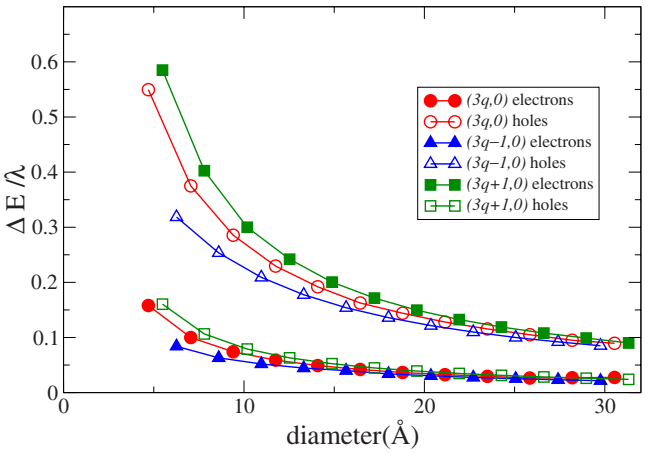

FIG. 2. (Color online) Normalized spin-orbit splitting of the top valence and bottom conduction bands as a function of the tube diameter for the three zigzag families.

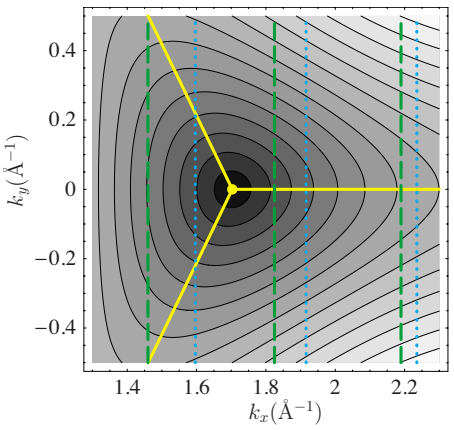

FIG. 3. (Color online) Contour plot of the graphene band structure calculated around the Fermi K point. The quantization lines corresponding to the (7,0) (green dashed line) and (8,0) (blue dotted line) CNTs closer to this point are also shown.

VB, whereas for NTs $(3q+1,0)$ the splitting is larger for the CB. In Fig. 1 we show one particular example of each of the three zigzag families, namely, the (8,0), the (9,0), and the (10,0) CNTs. Although our analysis concentrates on those bands closest to the Fermi level, it can be seen that the splitting of all other bands is also anisotropic and specific to each band. In particular, note that the second CB and VB show opposite behaviors to those of the bottom CB and the top VB (see below).

In Fig. 2 the SO energy splitting of the top valence and the bottom conduction bands is represented as a function of the tube diameter for the three zigzag CNT series, showing the family behavior described before.

The curvature effect is clearly seen: the SO energy splitting is much higher for CNTs with the smallest diameters; it can be noted as well how the differences among the three series decreases with increasing diameter. We have checked that the splitting is not negligible for larger NTs: for example, the (80,0) tube, with a diameter of 62.64 Å, which is roughly the same size of the CNT measured in Ref. 6, has a top VB normalized splitting of 0.04. An analogous family behavior of zigzag CNTs has been observed in other physical properties, such as the band gaps,[24–26] and it has been related to the trigonal warping effect. The three families can be understood by resorting to the zone-folding approach. Within this approximation, the energy bands of a general (n,m) CNT are given by imposing periodic boundary conditions to the graphene sheet: if the lines of allowed k vectors touch the Fermi points (K or K') of the hexagonal graphene BZ, the nanotube is a metal. This occurs when $n-m=3q$ with q as an integer; otherwise it is a semiconductor. The two semiconductor families, $n-m=3q\pm1$, correspond to nanotubes for which the quantization lines yielding the energy gap are at opposite sides of the Fermi point K (or K'). Thus, CNTs can be classified into three families: $n-m=3q+\nu$ with $\nu=0,\pm1$ being the so-called chiral index, hereafter referred as family index.[27] Denoting as K the BZ special point with coordinates $(\frac{4\pi}{3a},0)$, $\nu=-1$ has the closest quantization line yielding the gap to its left, over the ΓK line, whereas the $\nu=+1$ family has it to the right, over the KM line. Of course, if we choose the K' Fermi point to classify the nanotube families, the relative positions (right and left) of the quantization lines yielding the gap are reversed with respect to K. For simplicity, henceforth we will refer our discussion to the K point with coordinates given above.

In Fig. 3 we illustrate this general classification for the case of zigzag CNTs, with two examples belonging to different series. The allowed quantization lines of the (7,0) and the (8,0) tubes closer to K are shown over the graphene π-band-structure energy contour plot. The trigonal warping effect is clearly seen in these contours: quantization lines at opposite sides of K correspond to graphene bands with appreciably different slopes, although they are at similar distances. As the π graphene bands crossing at K have a different symmetry, the character of the conduction band changes from antibonding along the ΓK line to bonding along the KM line. Furthermore, the character of electron and hole bands is interchanged at the K point. This explains why tubes belonging to $\nu=\pm1$ families show an opposite behavior in their conduction (or valence) bands: the two bands closest to the Fermi energy have a different symmetry. In addition, it clarifies why in a given tube, as described above, the second VB (CB) has a reverse behavior with respect to the first VB (bottom CB): these second bands arise from quantization lines at opposite sides of K with respect to the first. Furthermore, the similar behavior of the metallic and the semiconductor $\nu=-1$ families can be explained by noticing that curvature effects shift the Fermi K point in Fig. 3 to the right, in such a way that the allowed quantization lines of the metallic tubes closer to K fall onto the same side as those corresponding to the $\nu=-1$ family.[23]

On the other hand, curvature changes the hybridization of the orbitals. The linear graphene bands crossing at K are of a pure π character around E_F; however, rehybridization of σ and π orbitals is very important for small radii nanotubes and is non-negligible in general. In order to show the σ-π hybridization of the zigzag nanotubes, we have calculated the contribution of each of the four orbitals forming the basis set for the valence- and conduction-band states closest in energy to the Fermi level at Γ; the results summed over all

TABLE I. Electronic densities.

	(8,0)		(9,0)		(10,0)	
Orbital	CB	VB	CB	VB	CB	VB
σ	0.057	0.087	0.058	0.103	0.121	0.061
π	0.943	0.913	0.941	0.897	0.879	0.939

the atoms of the unit cell are shown in Table I. NTs belonging to the $\nu=+1$ family have a larger contribution of the σ orbitals—that is, a larger σ-π rehybridization—in the conduction band than in the valence band; however, in tubes of the $\nu=0,-1$ families the σ-orbital density is larger in the valence band. Spin-orbit effects are more important for bands with larger curvature-induced rehybridization; therefore, curvature effects are responsible for the observed electron-hole anisotropic SO splitting. The different mixing of π and σ orbitals, due to the curvature of the tubes, was shown to affect the energy gaps of semiconducting nanotubes[24] with a similar family dependence. Here we have shown that it also influences the value of spin-orbit splitting in CNTs.

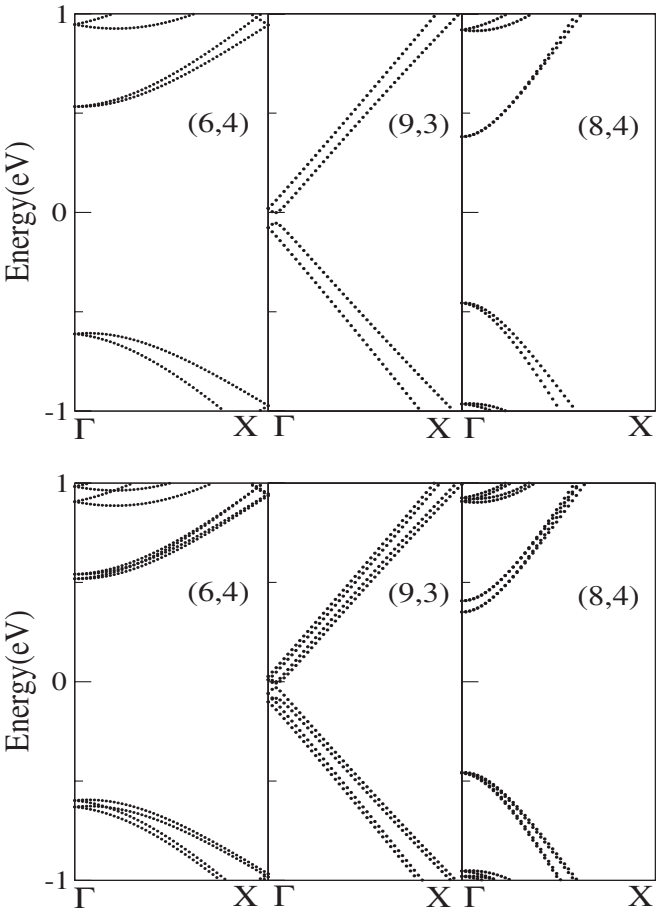

FIG. 4. Band structures around the Fermi level for three chiral CNTs: the (6,4) tube from the $\nu=-1$ family, the (9,3) primary metallic nanotube, and the (8,4) tube from the $\nu=+1$ family. The top panel shows results without SO effects; the bottom panel shows the bands calculated with SO coupling $\lambda=0.2$ eV.

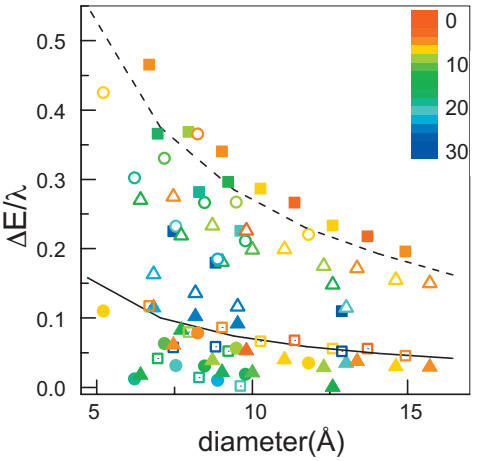

FIG. 5. (Color) Normalized energy-band splittings for chiral CNTs versus diameter. Squares stand for $\nu=+1$ family, triangles for $\nu-1$, and circles for $\nu=0$; full (open) indicate the top VB (bottom CB) splittings. Symbol color indicates the nanotube chiral angle. Full (dashed) line: bottom CB (top VB) splittings for metallic zigzag tubes.

B. Chiral tubes

We consider now chiral NTs (n,m) with $n\neq m\neq 0$ that do not have an inversion center. As mentioned above, curvature effects induce a shift of the Fermi wave vector k_F, opening a small gap at the Fermi energy in the primary metallic chiral CNTs, $(m-n)=3q$. But, in contrast to the results shown for achiral zigzag NTs, in both metal and semiconductor chiral NTs the SO interaction lifts all degeneracies.

The calculated energy splittings for these tubes follow the same behavior as those obtained for achiral zigzag CNTs: for tubes with $\nu=0$ $(n-m=3q)$ and $\nu=-1$ $(n-m=3q-1)$ the energy splitting is larger for the highest VB, while for tubes with $\nu=+1$ $(n-m=3q+1)$ the splitting is larger for the lowest CB. As an example for chiral tubes, the band structures calculated including the SOI for three particular tubes, (6,4), (9,3), and (8,4) belonging to each of the three families, are shown in Fig. 4.

However, chirality has an important effect in SOI: this is illustrated in Fig. 5, where the band splittings vs the diameter for chiral tubes belonging to the three families are depicted. The symbol color indicates the NT chiral angle. As a guide to the eye, the zigzag metallic $\nu=0$ results are also shown. It can be seen how chiral tubes follow the family behavior already described; notwithstanding, chirality effects introduce deviations from the zigzag monotonic behavior, due to the different orientation of the relevant quantization lines with respect to the K point. In general, the higher the chiral angle, the larger the deviation from the behavior of zigzag nanotubes.

IV. CONCLUSIONS

In summary, we have shown that spin-orbit induced splitting in carbon nanotubes is anisotropic and band dependent. The energy splittings induced by the SO interaction term are different for the highest valence band and the lowest conduc-

tion band depending on the tube family: for $\nu=0,-1$ the splitting is larger for the top valence band, whereas for tubes with $\nu=1$ the lowest conduction band has larger splitting. We have related the magnitude of the SO splitting with the σ-π hybridization induced by curvature, which is family dependent. The dissimilar σ-π hybridizations of the valence- and conduction-band states, which in turn depend on the position of the quantization lines yielding the gap with respect to the graphene K point, are the reason for the experimentally observed anisotropy in SO splitting in the absence of external fields. The natures of the NT electronic states and of the spin-orbit coupling have to be taken into account in order to understand the behavior of the electrons and the transport properties in the presence of applied fields. In particular, since a magnetic field breaks time-reversal symmetry, all degeneracies will be removed. The coupling of orbital and spin angular momenta induces a different slope in the energy vs magnetic field dependence of the electronic levels, as observed experimentally.[6] Therefore, SO effects should be considered in the modeling of CNT transport properties when a magnetic field is applied.

ACKNOWLEDGMENTS

We acknowledge fruitful discussions with A. Ayuela, J. I. Cerdá, and A. Ruiz. This work was partially supported by the Spanish DGES under Grants No. FIS2005-05478-C02-01, No. FIS2008-00124, No. MAT2006-05122, and No. MAT2006-06242.

[1] S. Sahoo, T. Kontoos, J. Furer, C. Hoffman, M. Gräber, A. Cottet, and C. Schönenberger, Nat. Phys. **1**, 99 (2005).
[2] L. W. Liu, J. H. Fang, L. Lu, H. F. Yang, A. Z. Jin, and C. Z. Gu, Phys. Rev. B **74**, 245429 (2006).
[3] L. Hueso, J. Pruneda, V. Ferrari, G. Burnell, J. Valdés-Herrera, B. Simmons, P. Littlewood, E. Artacho, A. Fert, and N. Mathur, Nature (London) **445**, 410 (2007).
[4] C. A. Merchant and N. Marković, Phys. Rev. Lett. **100**, 156601 (2008).
[5] P. Jarillo-Herrero, J. Kong, H. S. J. van der Zant, C. Dekker, L. P. Kouwenhoven, and S. De Franceschi, Phys. Rev. Lett. **94**, 156802 (2005).
[6] F. Kuemmeth, S. Ilani, D. Ralph, and P. McEuen, Nature (London) **452**, 448 (2008).
[7] P. Jarillo-Herrero, S. Sapmaz, C. Dekker, L. Kouwenhoven, and H. van der Zant, Nature (London) **429**, 389 (2004).
[8] L. Chico, M. P. López-Sancho, and M. C. Muñoz, Phys. Rev. Lett. **93**, 176402 (2004).
[9] Nanotubes are labeled by the numbers (n,m), given by the unrolled circumference vector $\boldsymbol{C}_h=n\boldsymbol{a}_1+m\boldsymbol{a}_2$ in the graphene lattice. $\boldsymbol{a}_1,\boldsymbol{a}_2$ are the two lattice vectors of graphene at 60°; $a=|\boldsymbol{a}_i|$.
[10] T. Ando, J. Phys. Soc. Jpn. **69**, 1757 (2000).
[11] M. V. Entin and L. I. Magarill, Phys. Rev. B **64**, 085330 (2001).
[12] A. De Martino, R. Egger, K. Hallberg, and C. A. Balseiro, Phys. Rev. Lett. **88**, 206402 (2002); A. De Martino, R. Egger, F. Murphy-Armando, and K. Hallberg, J. Phys.: Condens. Matter **16**, S1437 (2004).
[13] D. Huertas-Hernando, F. Guinea, and A. Brataas, Phys. Rev. B **74**, 155426 (2006).
[14] D. V. Bulaev, B. Trauzettel, and D. Loss, Phys. Rev. B **77**, 235301 (2008).
[15] T.-F. Fang, W. Zuo, and H.-G. Luo, Phys. Rev. Lett. **101**, 246805 (2008).
[16] C. L. Kane and E. J. Mele, Phys. Rev. Lett. **95**, 226801 (2005).
[17] J.-C. Charlier, X. Blase, and S. Roche, Rev. Mod. Phys. **79**, 677 (2007).
[18] J. C. Slater and J. F. Koster, Phys. Rev. **94**, 1498 (1954).
[19] D. Tománek and S. G. Louie, Phys. Rev. B **37**, 8327 (1988).
[20] D. J. Chadi, Phys. Rev. B **16**, 790 (1977).
[21] S. Gallego and M. C. Muñoz, Surf. Sci. **423**, 324 (1999).
[22] C. L. Kane and E. J. Mele, Phys. Rev. Lett. **78**, 1932 (1997).
[23] A. Kleiner and S. Eggert, Phys. Rev. B **63**, 073408 (2001).
[24] H. Yorikawa and S. Muramatsu, Phys. Rev. B **52**, 2723 (1995).
[25] R. Saito, G. Dresselhaus, and M. S. Dresselhaus, Phys. Rev. B **61**, 2981 (2000).
[26] T. Ando, J. Phys. Soc. Jpn. **74**, 777 (2005).
[27] The family index ν as defined in this work or, equivalently, $\mathrm{mod}(n-m,3)$, is called chiral index by other authors. Given that nanotubes with different chiralities may belong to the same family, we prefer the previous denomination.